European Journal of Radiology 110 (2019) 1–6

Contents lists available at ScienceDirect

European Journal of Radiology

journal homepage: www.elsevier.com/locate/ejrad

Research article

Dual-energy computed tomography for prediction of loco-regional recurrence after radiotherapy in larynx and hypopharynx squamous cell carcinoma

Houda Bahig[a,d,*], Andréanne Lapointe[a], Stéphane Bedwani[a], Jacques de Guise[b], Louise Lambert[a], Edith Filion[a], David Roberge[a], Laurent Létourneau-Guillon[c], Danis Blais[a], Sweet Ping Ng[d], Phuc Félix Nguyen-Tan[a]

[a] Radiation Oncology Department, Centre Hospitalier de l'Université de Montréal, Montreal, QC, Canada
[b] Centre de Recherche du CHUM, Centre Hospitalier de l'Université de Montréal, Montreal, QC, Canada
[c] Radiology Department, Centre Hospitalier de l'Université de Montréal, Montreal, QC, Canada
[d] Radiation Oncology Department, University of Texas MD Anderson Cancer Center, Houston, TX, United States

ARTICLE INFO

Keywords:
Dual-energy CT
Larynx cancer
Hypopharynx cancer
Iodine map
Radiomics
Loco-regional recurrence

ABSTRACT

Purpose: To investigate the role of quantitative pre-treatment dual-energy computed tomography (DECT) for prediction of loco-regional recurrence (LRR) in patients with larynx/hypopharynx squamous cell cancer (L/H SCC).

Methods: Patients with L/H SCC treated with curative intent loco-regional radiotherapy and that underwent treatment planning with contrast-enhanced DECT of the neck were included. Primary and nodal gross tumor volumes (GTVp and GTVn) were contoured and transferred into a Matlab® workspace. Using a two-material decomposition, GTV iodine concentration (IC) maps were obtained. Quantitative histogram statistics (maximum, mean, standard deviation, kurtosis and skewness) were retrieved from the IC maps. Cox regression analysis was conducted to determine potential predictive factors of LRR.

Results: Twenty-five patients, including 20 supraglottic and 5 pyriform sinus tumors were analysed. Stage I, II, III, IVa and IVb constituted 4% (1 patient), 24%, 36%, 28% and 8% of patients, respectively; 44% had concurrent chemo-radiotherapy and 28% had neodjuvant chemotherapy. Median follow-up was 21 months. Locoregional control at 1 and 2 years were 75% and 69%, respectively. For the entire cohort, GTVn volume (HR *1.177* [*1.001-1.392*], p = 0.05), voxel-based maximum IC of GTVp (HR 1.099 [95% CI: 1.001–1.209], p = 0.05) and IC standard deviation of GTVn (HR 9.300 [95% CI: 1.113–77.725] p = 0.04) were predictive of LRR. On subgroup analysis of patients treated with upfront radiotherapy +/- chemotherapy, both voxel-based maximum IC of GTVp (HR 1.127 [95% CI: 1.010–1.258], p = 0.05) and IC kurtosis of GTVp (HR 1.088 [95% CI: 1.014–1.166], p = 0.02) were predictive of LRR.

Conclusion: This exploratory study suggests that pre-radiotherapy DECT-derived IC quantitative analysis of tumoral volume may help predict LRR in L/H SCC.

1. Introduction

In the last decades, treatment approaches for larynx and hypopharynx squamous cell carcinoma (L/H SCC) have shifted toward organ-preserving strategies, with the aim of limiting functional impairments associated with total laryngectomy/pharyngolaryngectomy and improving patients' quality of life [1]. While organ-preserving trials have provided strong evidence that well-selected patients with L/H SCC may benefit from organ-preservation strategies, there remains substantial controversy on the optimal management of these patients [2]. In fact, despite improvement in radiotherapy techniques and systemic treatments, relapse rates in locally advanced L/H SCC after organ-preserving treatment remain high, with rates of loco-regional recurrence (LRR) at 5 years reaching 30–40% [3–5]. In addition, observational data suggest that 5-year survival rates of L/H SCC have decreased [6].

Better tumor characterisation through use of imaging biomarkers has the potential to provide insightful information for outcome

* Corresponding author at: Department of Radiation Oncology, 1000 Saint-Denis, Montreal, Quebec, H2X 0C1, Canada.
E-mail address: houda.bahig.chum@ssss.gouv.qc.ca (H. Bahig).

https://doi.org/10.1016/j.ejrad.2018.11.005
Received 18 May 2018; Received in revised form 28 October 2018; Accepted 4 November 2018

prediction and treatment selection in L/H SCC. Various functional imaging modalities assessing tumor metabolism, hypoxia, cellularity and perfusion have been investigated in HNC. These modalities notably comprise the use of positron emission tomography (PET), including 18F- fluorodeoxyglucose (FDG-PET) [7–9], 18F-fluoromisonidazole-PET (FMISO-PET) [8,10] or 18-F-fluoroazomycin arabinoside-PET (FAZA-PET) [11]; use of magnetic resonance imaging (MRI), including diffusion weighted imaging [12,13] or dynamic contrast-enhance MRI [11,12]; as well as use of CT perfusion imaging [14,15]. Assessment of tumor perfusion in HNC is considered a useful tool for non-invasive evaluation of intra-tumoral microvessel density and for characterisation of tumor angiogenesis [16,17].

Dual-energy computed tomography (DECT) is an advanced form of CT in which image acquisition is performed at 2 different energies. This technology allows tissue characterisation through material decomposition and voxel-to-voxel determination of iodine concentration, which can be used to derive a regional blood volume map [18,19]. The applications of DECT in head and neck cancer have been a growing area of interest, with several recent studies showing the benefit of iodine characterisation and virtual monoenergetic images for detection and delineation of head and neck tumor [20,21], differentiation between metastatic, inflammatory and benign cervical lymph nodes [22,23] or assessment of cartilage invasion [24,25]. However, the role of DECT-derived quantitative imaging to predict oncological outcomes in HNC has never been previously investigated. Yet the rich quantitative information provided by DECT offers a unique opportunity for functional biomarker analysis. As previously proposed in single energy CT studies [26], we hypothesized that higher tumor iodine content is indicative of increased blood volume and capillary hyperpermeability associated with neo-angiogenesis. The purpose of this study was to investigate the role of DECT-derived quantitative histogram analysis of pre-treatment for prediction of LRR in patients with L/H SCC.

2. Material and methods

2.1. Patient population

Patients with larynx or hypopharynx cancer treated with radiotherapy and that underwent a pre-treatment planning DECT between January 2015 and August 2016 at our institution, were included in this retrospective study. Inclusion criteria were: [1] histological diagnosis of SCC of the larynx or hypopharynx [2]; curative intent locoregional radiotherapy +/- concurrent chemotherapy; [3] pre-treatment contrast-enhanced planning DECT of the neck. Patients that received induction chemotherapy and had residual disease at time of radiotherapy were included. Patients with early stage (T1-T2N0) glottic cancers were excluded. All cases were discussed in the context of a multidisciplinary tumor board. The protocols and patient consent forms were reviewed and approved by our institutional ethics committee.

2.2. DECT and radiotherapy planning

All patients had a 1.5 mm slice thickness planning dual-energy computed tomography (SOMATOM Definition Flash; Siemens Healthineers) from the vertex to the carina with and without intravenous contrast injection in supine position. Immobilisation device included a thermoplastic mask of the head and shoulders fixed to the treatment table. Iohexol contrast bolus was injected (Omnipaque 240 mg/ml) in the antecubital vein at a rate of 2.2 ml/second. Scan delay was determined based on scan duration, injection duration and bolus tracking, and yielded on average a total a volume of contrast between 45–50 ml. Immediately after, 40 ml saline solution was sequentially injected at a rate of 2.2 ml/second. DECT was acquired 5 s after contrast bolus tracking in the common carotid artery, in order to ensure image acquisition during the arterial phase and eliminate variation in cardiac output between patients. Two sets of spiral CT data were simultaneously acquired with the following parameters: slice thickness of 2 mm, pitch of 0.55, rotation time of 0.28 s, collimation of 64 x 0.6 mm and X-ray tube potentials of 100 kVp and 140Sn kVp (Sn = additional tin filtration), a matrix of 512 × 512 pixels, a field of view of 50 cm and a voxel size of 1 × 1 × 1 mm [3]. A Q30 filter kernel was used for image reconstruction. Tube current modulation was used in for individual radiation dose optimization. Patients were requested not to swallow during DECT acquisition. Sequential acquisition of a non-contrast injected CT scan allowed for systematic verification of larynx position to ensure that the patient did not swallow during the examination. Primary gross tumor volume (GTVp) and nodal gross tumor volume (GTVn) were contoured at time of treatment planning on the average- weighted DECT image by the treating radiation oncologist. A planning positron tomography (PET)-CT (available in 40% of patients) and/or a magnetic resonance imaging (available in 92% of patients) fused with planning CT could be used to verify tumor volume or help decision making regarding tumor delineation in cases where the tumor edge was not clearly visualised on DECT. Tumor contours were systematically reviewed and approved by a minimum of 2 radiation oncologists in the context of the routine quality assurance process of radiation treatment planning.

Patients were treated with volumetric arc modulated radiotherapy (RapidArc®, Varian Medical Systems, Palo Alto, CA) using 6-MV photons. Patients undergoing definitive radiotherapy +/- concurrent chemotherapy were treated to a dose to 70 Gy in 35 fractions to the gross disease, 60 Gy in 30 fractions to high risk nodal region and 50 Gy in 25 fractions to low risk nodal region, given in 5 daily fractions per week. Treatment plans were normalised so that the prescription dose covered at least 95% of the PTV volume. Eclipse TPS (Varian Medical Systems, Palo Alto, CA) with Analytical Anisotropic Algorithm was used for dose calculation.

2.3. DECT-derived iodine concentration map and histogram analysis

Primary gross tumor volume (GTVp) and nodal gross tumor volume (GTVn) were transferred on a MIM Maestro workstation (MIM Software Inc., Cleveland, OH) where the contours were subsequently visually verified on the 100 kV and 140 kV series by a radiation oncologist and modified to carefully exclude: air, bone, cartilage, peripheral fat. All DECT were examined visually to ensure absence of motion or streak artefacts. Using an in-house script (Matlab — MathWorks, Natick, MA), iodine concentration (in mg/ml) was extracted from GTVp and GTVn structures by determining the iodine partial electron density from each voxel, using a two-material decomposition method previously described by our group [27] and based on principal component analysis called eigentissue decomposition [28]. Fig. 1 shows an example of GTVp and GTVn contours along with the corresponding iodine maps from a patient with locally advanced hypopharynx SCC. Quantitative histogram analysis was performed to retrieve statistics from GTVp and GTVn iodine maps.

2.4. Follow-up and statistics

Patients had alternating follow-up by their otolaryngologist and radiation-oncologist every 2 months for the first 2 years and every 4 months for the following 3 years. Every patient had a follow-up CT scan at 6–8 weeks after treatment and as well as anytime symptoms and/or results on physical examination were suspicious for recurrence. LRR was detected on clinical examination and/or CT scan ± 18-fluorodeoxyglucose positron emission tomography and confirmed histologically. Follow-up duration was defined from the date of treatment completion to the date of last follow-up or death. Kaplan–Meier method was used for estimation of locoregional control and relapse free survival (RFS). Univariate Cox regression analysis was performed to determine predictors of LRR, with p values $p \leq 0.05$ considered statistically significant. Descriptive statistics retrieved from iodine concentration

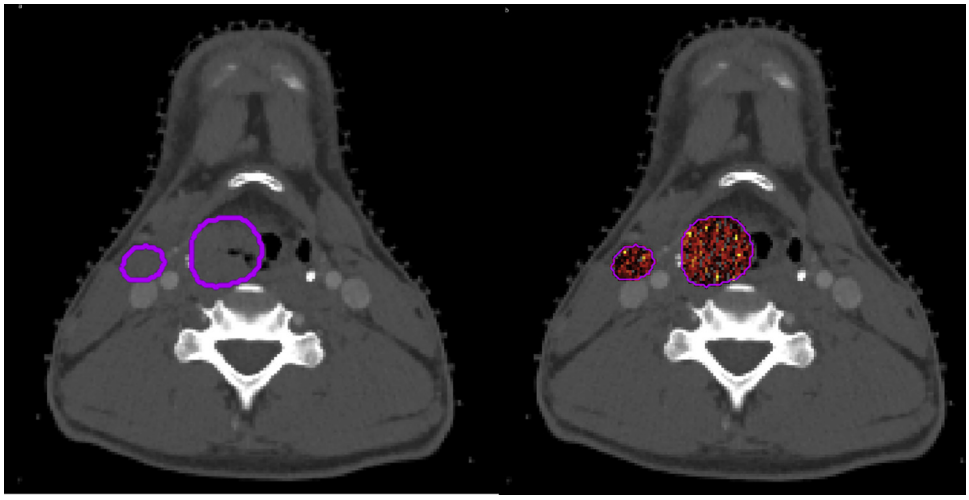

Fig. 1. Axial slice of weighted-average DECT from a patient with locally advanced hypopharynx squamous cell cancer. Legend: Primary and nodal GTV are shown (pink contours) (a), along with their corresponding fused iodine maps (a).

included maximum, mean, standard deviation, kurtosis and skewness. Clinical factors such as age, gender, tumor site, smoking status, stage, GTVp and GTVn volumes were also analyzed. SPSS 24 (IBM, Armonk, NY) was used for statistical analysis.

3. Results

3.1. Patients and treatments characteristics

In total, 25 patients met inclusion criteria. Twenty-five patients, including 20 supraglottic and 5 pyriform sinus tumors were analysed; 76% were male. Median age was 65 years (43–79). Median GTVp volume was 7.9 cm^3 (range = 0.7–51.8 cm^3) and median GTVn volume was 7.0 cm^3 (range = 0.5–25.8 cm^3). Stage I, II, III, IVa and IVb constituted 4% (1 patient), 24%, 36%, 28% and 8% of patients, respectively. Forty-four percent had concurrent cisplatin and 28% had neoadjuvant chemotherapy consisting of docetaxel-cisplatin or paclitaxel-carboplatin. Patients and treatment characteristics are summarized in Table 1.

3.2. Treatment outcomes

The median follow-up time was 21 months (range: 9–34 months). Relapse patterns were as follow: 4 patients presented isolated local recurrence, 1 patient had synchronous local and regional recurrence, 1 patient had synchronous regional and distant recurrence, and 1 had isolated distant metastasis. Actuarial LRR at 1 and 2 years was 75% and 69% (Fig. 2). Actuarial RFS at 1 and 2 years was 70% and 64% (Fig. 3).

3.3. Predictors of LRR

Table 2 presents univariate Cox regression analysis for risk of LRR for the entire cohort, while Table 3 presents univariate Cox regression analysis for risk of LRR for the subgroup of patients treated with upfront radiation +/- concurrent chemotherapy. For the entire cohort, GTVn volume (HR *1.177* [*1.001-1.392*], p = 0.05), maximum IC of GTVp (HR 1.099 [95% CI: 1.001–1.209], p = 0.05) and IC standard deviation of GTVn (HR 9.300 [95% CI: 1.113–77.725] p = 0.04) were predictive of LRR (Table 2). On subgroup analysis of patients treated with upfront radiotherapy +/- chemotherapy, both maximum IC of GTVp (HR 1.127 [95% CI: 1.010–1.258], p = 0.05) and IC kurtosis of GTVp (HR 1.088 [95% CI: 1.014–1.166], p = 0.02) were predictive of LRR (Table 3).

Table 1
Patients and tumors' characteristics.

Age; median (range)	65 (43-79)
Gender	
Female	6 (24%)
Male	19 (76%)
Subsite	
Larynx	20 (80%)
Hypopharynx	5 (20%)
Active Smoker	
Yes	7 (28%)
No	18 (72%)
T stage	
T1	16%
T2	44%
T3	40%
N stage	
N0	11 (44%)
N1	5 (20%)
N2	7 (28%)
N3	2 (8%)
GTVp volume; cm^3 (median; range)	7.9 (0.7-51.8)
GTVn volume (N = 14); cm^3 (median; range)	7.0 (0.5-25.8)
Concurrent chemotherapy	13 (52%)
Neoadjuvant chemotherapy	7 (28%)

IHC = Immunohistochemistry; GTVp = Primary gross tumor volume; GTVn = nodal gross tumor volume.

4. Discussion

This pilot study explores the role of DECT-derived quantitative imaging for outcome prediction in HNC. In this study, we describe a method allowing for volumetric extraction of iodine fraction from each voxel of the primary tumor and involved lymph nodes in L/H SCC. Iodine concentration was used as a surrogate for regional blood volume, with the working hypothesis that increased tumor angiogenesis would result in higher iodine contrast enhancement, as previously supported in single energy CT studies [26]. In our pilot cohort of 25 patients, higher maximum IC of the primary tumor as well as higher volume and IC standard deviation of involved lymph nodes were predictive of LRR in L/H SCC. In the subgroup of patients treated with upfront radiation +/- concurrent chemotherapy, both higher maximum IC and higher IC kurtosis of the primary tumor were predictive of cancer relapse. While the prognostic value of nodal tumor volume has previously been reported [29], this preliminary study suggests that DECT-derived iodine map histogram metrics have the potential to provide easily accessible

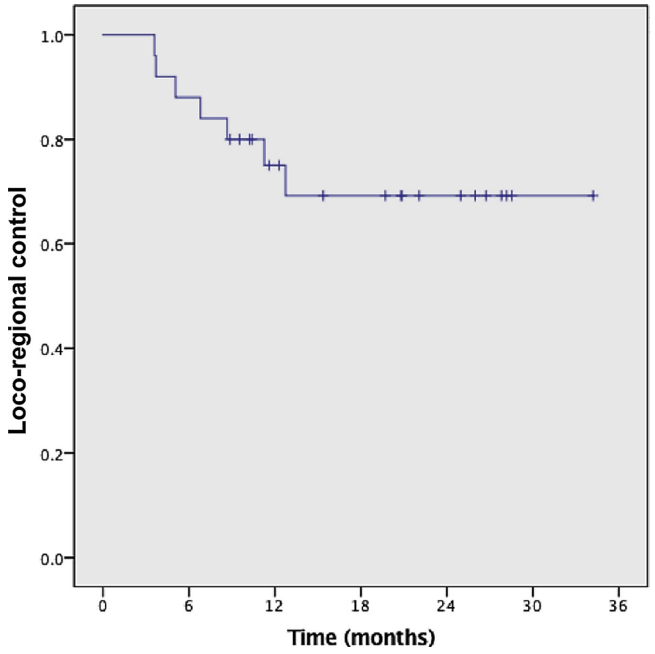

Fig. 2. Kaplan Meier curves of loco-regional control as a function of time.

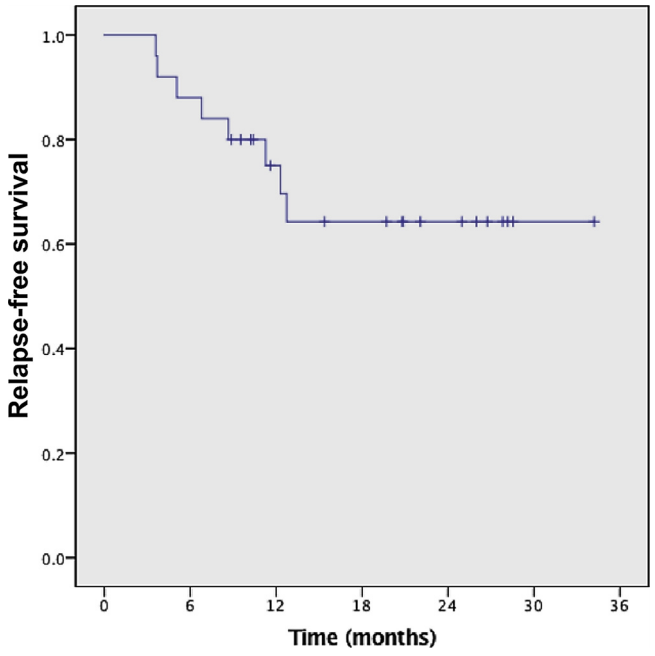

Fig. 3. Kaplan Meier curves of relapse-free survival as a function of time.

information that can be valuable for tumor characterization, outcome prediction, treatment selection and dose painting. Contrary to oropharynx cancer where prognostic factors such as p16 status have been widely recognized, there are limited markers that help us predict LRR in L/H cancers.

DECT is an advanced imaging technique allowing for acquisition of 2 series of CT images at different energies. Based on the principle of energy-dependant photoelectric effect, precise tissue characterisation and quantification of different materials such as iodine can be achieved [30]. DECT offers a unique opportunity for analysis of imaging biomarker; however, in current literature, its use for outcome prediction is generally unexplored. In one study focusing on assessment of iodine content of cervical neck nodes, Tawfik et al. [23] reported that lower mean iodine content derived from DECT could differentiate metastatic

Table 2
Univariate Cox regression analysis of all variables for risk of LRR for entire cohort.

	LRR	No LRR	HR (95% CI)	p
Clinical features				
Male (vs. Female) (%)	71%	72%	0.881 (0.171-4.549)	0.8
Age; M (y)	60	64	0.975 (0.910-1.044)	0.4
Active smoker (vs. Non smoker) (%)	43%	22%	2.435 (0.542-10.938)	0.4
T3 (vs. T1-2) (%)	29%	44%	0.744 (0.327-1.695)	0.6
N+ (vs. N0) (%)	57%	56%	1.276 (0.283-5.743)	0.8
Hypopharynx (vs. Larynx) (%)	29%	28%	1.258 (0.537-2.945)	0.6
Volume GTVp; M (cm^3)	11.5	6.5	1.035 (0.981-1.091)	0.2
Volume GTVn; M (cm^3)	***11.4***	***5.2***	***1.177 (1.001-1.392)***	***0.05***
GTVp histogram analysis				
IC max; M (mg/ml)	***21.0***	***16.1***	***1.099 (1.001-1.209)***	***0.05***
IC max 99 percentile; M (mg/ml)	8.5	8.2	1.01 (0.780-1.307)	0.9
IC mean; M (mg/ml)	1.9	1.6	1.977 (0.708-5.226)	0.2
IC SD; M (mg/ml)	2.1	1.9	1.367 (0.440-4.248)	0.6
IC skewness; M (mg/ml)	2.0	2.1	0.993 (0.562-1.756)	0.9
IC kurtosis; M (mg/ml)	17.8	13.2	1.009 (0.980-1.039)	0.5
GTVn histogram analysis (N = 14)				
IC max; M (mg/ml)	10.5	7.6	1.226 (0.908-1.655)	0.2
IC max 99 percentile; M (mg/ml)	6.6	4.1	1.526 (0.997-2.336)	0.06
IC mean; M (mg/ml)	1.5	1.8	0.967 (0.512-1.827)	0.9
IC SD; M (mg/ml)	***1.6***	***1.1***	***9.300 (1.113-77.725)***	***0.04***
IC skewness; M (mg/ml)	1.2	0.9	1.461 (0.278-7.694)	0.7
IC kurtosis; M (mg/ml)	4.4	4.7	0.907 (0.481-1.712)	0.8

HR= Hazard ratio; CI = confidence interval; LRR = loco-regional recurrence; N+= node positive disease; M = mean; IC = iodine concentration; N = number; max= maximum; SD= standard deviation.

Table 3
Cox regression analysis for risk of LRR for subgroup of patients treated with upfront radiation +/- chemotherapy (N = 17).

	LRR	No LRR	HR (95% CI)	p
Clinical features				
Male (vs. Female); (%)	57%	58%	0.907 (0.388-2.123)	0.8
Age; M (y)	59	63	0.978 (0.912-1.049)	0.5
Active smoker (vs. Non smoker) (%)	50%	17%	5.010 (0.901-27.863)	0.06
T3 (vs. T1-2); (%)	17%	33%	0.602 (0.205-1.772)	0.4
N+ (vs. N0) (%)	50%	42%	1.168 (0.233-5.857)	0.8
Hypopharynx (vs. Larynx) (%)	17%	17%	1.053 (0.359-3.089)	0.9
Volume GTVp; M (cm^3)	12.7	6.8	1.022 (0.970-1.076)	0.4
Volume GTVn; M (cm^3)	13.8	3.9	1.159 (0.983-1.1366)	0.08
GTVp histogram analysis				
IC max; M (mg/ml)	***23.0***	***16.1***	***1.127 (1.010 1.258)***	***0.03***
IC max 99 percentile; M (mg/ml)	9.2	6.1	1.160 (0.876-1.538)	0.3
IC mean; M (mg/ml)	2.0	1.8	1.736 (0.504-5.978)	0.4
IC SD; M (mg/ml)	2.3	1.6	*1.120 (0.348 3.612)*	*0.8*
IC skewness; M (mg/ml)	2.1	1.6	1.640 (0.705 3.815)	0.2
IC kurtosis; M (mg/ml)	***19.4***	***8.1***	***1.088 (1.014 1.166)***	***0.02***
GTVn histogram analysis (N = 9)				
IC max; M (mg/ml)	14.3	8.3	1.264 (0.865-1.846)	0.2
IC max 99 percentile; M (mg/ml)	6.9	4.5	1.397 (0.875-2.085)	0.2
IC mean; M (mg/ml)	1.6	2.6	0.775 (0.311-1.930)	0.8
IC SD; M (mg/ml)	1.8	1.1	3.682 (0.775-17.499)	0.1
IC skewness; M (mg/ml)	1.2	0.6	5.358 (0.078-366.072)	0.4
IC kurtosis; M (mg/ml)	4.3	4.1	1.244 (0.335-4.622)	0.7

HR= Hazard ratio; CI = confidence interval; LRR = loco-regional recurrence; N+ = node positive disease; M = mean; IC = iodine concentration; N = number; max = maximum; SD= standard deviation.

SCC from normal or inflammatory lymph nodes. Unlike our study, iodine content measurements were limited to a region of interest in the axial section and only mean and standard deviation values of iodine content were reported. In a study by Kuno et al. [24], the combination of weighted average and iodine overlay images was found to improve the diagnostic performance and inter-observer reproducibility of laryngeal cartilage invasion assessment from HNC SCC [24]. In lung cancer, Schmidt-Binder et al. [31] reported a strong correlation between maximum standardized uptake value of 18- fluorodeoxyglucose positron emission tomography (18FDG-PET)/CT and maximum iodine-related attenuation on DECT for both primary tumours and involved thoracic lymph nodes of non-small cell lung cancer. The latter study suggests an association between metabolic activity and perfusion and is in concordance with our findings that maximum tumoral IC is associated with worse outcomes.

Perfusion imaging as a surrogate of angiogenesis and predictor of oncological outcomes has previously been largely studied in HNC but results have generally been conflicting [32–36]. On one hand, several studies have reported an association between increased tumor perfusion and improved treatment response, supporting that poor tumor perfusion induces hypoxia and radioresistance [32,37]. On the other hand, other studies have supported a correlation between elevated perfusion, tumor recurrence and metastatic potential, suggesting that highly perfused tumors may present a more aggressive biology [36,38]. Pietch et al. [38] reported significantly higher pre-treatment CT-derived perfusion metrics in recurrent HNC tumors. Similarly, using PET with oxygen-15-labeled water for assessment of blood flow, Lehtio et al. reported poor local control after radiotherapy and decreased survival in tumors with higher pre-treatment blood flow [36]. These studies support the hypothesis that high perfusion may rather be a consequence of the neovascularization induced by hypoxia [39,40]. Discrepancies on the prognostic value of perfusion can be in part explained by the combination of various HNC tumors subsites which does not allow to account for the heterogeneous biology of individual tumours. Interestingly, a study by the Memorial Sloan Kettering Cancer Center recently reported on dual assessment of tumor hypoxia and perfusion in 120 HNC patients that underwent 18F-FMISO-PET. In this study, both positive and negative correlation between hypoxia and perfusion were observed for individual lesions [8], supporting that both scenarios are possible and likely vary based on tumor biology. In addition, an association between angiogenesis and glucose metabolism was also supported by positive correlation shown between maximum standardized uptake value on PET and perfusion in moderately large (stage T2–3) HNC tumors [41]. Increasing level of evidence suggests that perhaps quantification of heterogeneity of tumors perfusion is key in understanding inter- and intra-tumour phenotypes as well as in predicting HNC outcomes [42]. This is also supported by findings from our study where higher IC kurtosis (representing peakedness of the shape of the probability distribution) of primary tumor and higher IC standard deviation (reflecting dispersion of the histogram) of involved lymph nodes were found to be potential biomarkers. To this effect, DECT-derived iodine map histogram metrics offer an opportunity for better quantification of tumour perfusion heterogeneity, as a window to individual phenotypes of HNC tumors.

Non-invasive assessment of microvessel density for prediction of oncological outcomes has been reported in multiple studies using perfusion CT [14,16,43] or DCE-MRI [44,45]. While perfusion CT measures variations in tissue attenuation as the contrast is dynamically administered, DCE-MRI measures variations in signal intensity. Both modalities have the potential to provide more useful and more complete information in regards to tumor perfusion in comparison to the static iodine map provided by the DECT, notably a larger range of metrics such as blood flow, blood volume, mean transit time, and permeability values. Comparatively, another disadvantage of static DECT iodine map is the uncertainty around the time of acquisition for optimal assessment of iodine contrast within the tumor. However, with these limitations in mind, there are several advantages of the static DECT, which still makes it a potentially valuable tool in the clinic. In the particular context of radiotherapy, the static examination makes it possible to derive iodine map directly from the injected planning scan (obtained for all patients), therefore providing functional information without the need for a supplementary examination and an added image co-registration step as part of the radiotherapy planning workflow. Additional advantages of this method include reduced radiation dose compared to dynamic CT as well. Finally, the shorter acquisition time of DECT iodine map makes this examination at reduced risk of motion artefact in comparison to dynamic MRI or CT. Given the increasing number of radiotherapy facilities acquiring DECT technology for its improved precision of dose calculation [46], this method has the potential to be integrated widely as part of the head and neck radiotherapy planning workflow.

Our study aimed at assessing the feasibility of using DECT-derived IC maps for clinical outcome prediction. This study is limited by its small sample size as well as by its heterogeneous cohort of patients. In fact, although our cohort has the advantage of focusing on L/H SCC exclusively, patients with mixed cancer stages and mixed treatment modalities were included. As it is possible that induction chemotherapy induced iodine map alteration that may have affected the validity of our results, we proceeded to a subgroup analysis of patients treated with upfront radiotherapy +/- chemotherapy, with similar findings in regards to maximum GTVp IC, in addition to GTVp kurtosis of iodine map. In addition, another important limitation of our study is that only voxel-based maximum iodine concentration was associated with risk of LRR, but not 99 iodine concentration percentile. Voxel-based maximum iodine concentration value is more vulnerable to noise compared to use of a larger region of interest such as 99 iodine concentration percentile. Preliminary findings of our study warrant further validation in a larger cohort. Due to the small sample size and exploratory nature of the study, only a univariate analysis of potential predictive factors of LRR was conducted.

In conclusion, we used pre-radiotherapy DECT-derived IC quantitative analysis, as a potential surrogate of microvessel density and heterogeneity of perfusion. The described method is a promising tool for outcome prediction in L/H SCC. Maximum IC and IC kurtosis of primary tumor, as well as IC standard deviation of involved lymph node are readily available imaging biomarkers that can be derived from pre-treatment diagnostic or planning DECT and that may help predict LRR in L/H SCC. Validation of the predictive value of these biomarkers in a larger cohort of patients is required.

Conflicts of interest

This work was supported by Fonds de Recherche du Québec-Santé. Houda Bahig, Edith Filion and David Roberge received research grant from Varian Medical Systems, unrelated to current work. Houda Bahig and David Roberge received speakers Honoraria from Siemens Healthineers/Varian Medical Systems, unrelated to current work.

References

[1] J.L. Lefebvre, K.K. Ang, Larynx preservation clinical trial design: key issues and recommendations-a consensus panel summary, Int. J. Radiat. Oncol. Biol. Phys. 73 (5) (2009) 1293–1303.
[2] M. Riga, L. Chelis, V. Danielides, T. Vogiatzaki, T.L. Pantazis, D. Pantazis, Systematic review on T3 laryngeal squamous cell carcinoma; still far from a consensus on the optimal organ preserving treatment, Eur. J. Surg. Oncol. 43 (1) (2017) 20–31.
[3] A.A. Forastiere, H. Goepfert, M. Maor, T.F. Pajak, R. Weber, W. Morrison, et al., Concurrent chemotherapy and radiotherapy for organ preservation in advanced laryngeal cancer, N. Engl. J. Med. 349 (22) (2003) 2091–2098.
[4] J.L. Lefebvre, G. Andry, D. Chevalier, B. Luboinski, L. Collette, L. Traissac, et al., Laryngeal preservation with induction chemotherapy for hypopharyngeal squamous cell carcinoma: 10-year results of EORTC trial 24891, Ann. Oncol. 23 (10) (2012) 2708–2714.
[5] A.A. Forastiere, Q. Zhang, R.S. Weber, M.H. Maor, H. Goepfert, T.F. Pajak, et al.,

Long-term results of RTOG 91-11: a comparison of three nonsurgical treatment strategies to preserve the larynx in patients with locally advanced larynx cancer, J. Clin. Oncol. 31 (7) (2013) 845–852.
[6] R.L.M.K. Siegel, A. Jemal, Cancer statistics, CA Cancer J. Clin. 66 (2016) 7–30.
[7] L. Preda, G. Conte, L. Bonello, C. Giannitto, L.L. Travaini, S. Raimondi, et al., Combining standardized uptake value of FDG-PET and apparent diffusion coefficient of DW-MRI improves risk stratification in head and neck squamous cell carcinoma, Eur. Radiol. 26 (12) (2016) 4432–4441.
[8] M. Grkovski, H. Schoder, N.Y. Lee, S.D. Carlin, B.J. Beattie, N. Riaz, et al., Multiparametric Imaging of Tumor Hypoxia and Perfusion with (18)F-Fluoromisonidazole Dynamic PET in Head and Neck Cancer, J. Nucl. Med. 58 (7) (2017) 1072–1080.
[9] M. Bogowicz, O. Riesterer, L.S. Stark, G. Studer, J. Unkelbach, M. Guckenberger, et al., Comparison of PET and CT radiomics for prediction of local tumor control in head and neck squamous cell carcinoma, Acta Oncol. 56 (11) (2017) 1531–1536.
[10] P. Dirix, V. Vandecaveye, F. De Keyzer, S. Stroobants, R. Hermans, S. Nuyts, Dose painting in radiotherapy for head and neck squamous cell carcinoma: value of repeated functional imaging with (18)F-FDG PET, (18)F-fluoromisonidazole PET, diffusion-weighted MRI, and dynamic contrast-enhanced MRI, J. Nucl. Med. 50 (7) (2009) 1020–1027.
[11] L.S. Mortensen, J. Johansen, J. Kallehauge, H. Primdahl, M. Busk, P. Lassen, et al., FAZA PET/CT hypoxia imaging in patients with squamous cell carcinoma of the head and neck treated with radiotherapy: results from the DAHANCA 24 trial, Radiother. Oncol. 105 (1) (2012) 14–20.
[12] S. Chawla, S. Kim, L. Dougherty, S. Wang, L.A. Loevner, H. Quon, et al., Pretreatment diffusion-weighted and dynamic contrast-enhanced MRI for prediction of local treatment response in squamous cell carcinomas of the head and neck, AJR Am. J. Roentgenol. 200 (1) (2013) 35–43.
[13] M. Lambrecht, B. Van Calster, V. Vandecaveye, F. De Keyzer, I. Roebben, R. Hermans, et al., Integrating pretreatment diffusion weighted MRI into a multivariable prognostic model for head and neck squamous cell carcinoma, Radiother. Oncol. 110 (3) (2014) 429–434.
[14] R. Hermans, M. Meijerink, W. Van den Bogaert, A. Rijnders, C. Weltens, P. Lambin, Tumor perfusion rate determined noninvasively by dynamic computed tomography predicts outcome in head-and-neck cancer after radiotherapy, Int. J. Radiat. Oncol. Biol. Phys. 57 (5) (2003) 1351–1356.
[15] A.A. Razek, A.M. Tawfik, L.G. Elsorogy, N.Y. Soliman, Perfusion CT of head and neck cancer, Eur. J. Radiol. 83 (3) (2014) 537–544.
[16] L. Ash, T.N. Teknos, D. Gandhi, S. Patel, S.K. Mukherji, Head and neck squamous cell carcinoma: CT perfusion can help noninvasively predict intratumoral microvessel density, Radiology 251 (2) (2009) 422–428.
[17] S. Ling, D. Deng, Y. Mo, X. Zhang, X. Guan, Q. Wei, Correlations between CT perfusion parameters and vascular endothelial growth factor expression and microvessel density in implanted VX2 lung tumors, Cell Biochem. Biophys. 70 (1) (2014) 629–633.
[18] R. Forghani, A. Srinivasan, B. Forghani, Advanced tissue characterization and texture analysis using dual-energy computed tomography: horizons and emerging applications, Neuroimaging Clin. N. Am. 27 (3) (2017) 533–546.
[19] T.J. Vogl, B. Schulz, R.W. Bauer, T. Stover, R. Sader, A.M. Tawfik, Dual-energy CT applications in head and neck imaging, AJR Am. J. Roentgenol. 199 (5 Suppl) (2012) S34–9.
[20] M.H. Albrecht, J.E. Scholtz, J. Kraft, R.W. Bauer, M. Kaup, P. Dewes, et al., Assessment of an Advanced Monoenergetic Reconstruction Technique in Dual-Energy Computed Tomography of Head and Neck Cancer, Eur. Radiol. 25 (8) (2015) 2493–2501.
[21] M. Toepker, C. Czerny, H. Ringl, J. Fruehwald-Pallamar, F. Wolf, M. Weber, et al., Can dual-energy CT improve the assessment of tumor margins in oral cancer? Oral Oncol. 50 (3) (2014) 221–227.
[22] A. Srinivasan, R.A. Parker, A. Manjunathan, M. Ibrahim, G.V. Shah, S.K. Mukherji, Differentiation of benign and malignant neck pathologies: preliminary experience using spectral computed tomography, J. Comput. Assist. Tomogr. 37 (5) (2013) 666–672.
[23] A.M. Tawfik, A.A. Razek, J.M. Kerl, N.E. Nour-Eldin, R. Bauer, T.J. Vogl, Comparison of dual-energy CT-derived iodine content and iodine overlay of normal, inflammatory and metastatic squamous cell carcinoma cervical lymph nodes, Eur. Radiol. 24 (3) (2014) 574–580.
[24] H. Kuno, H. Onaya, R. Iwata, T. Kobayashi, S. Fujii, R. Hayashi, et al., Evaluation of cartilage invasion by laryngeal and hypopharyngeal squamous cell carcinoma with dual-energy CT, Radiology 265 (2) (2012) 488–496.
[25] R. Forghani, M. Levental, R. Gupta, S. Lam, N. Dadfar, H.D. Curtin, Different spectral hounsfield unit curve and high-energy virtual monochromatic image characteristics of squamous cell carcinoma compared with nonossified thyroid cartilage, AJNR Am. J. Neuroradiol. 36 (6) (2015) 1194–1200.
[26] K.A. Miles, Tumour angiogenesis and its relation to contrast enhancement on computed tomography: a review, Eur. J. Radiol. 30 (3) (1999) 198–205.
[27] A. Lapointe, A. Lalonde, H. Bahig, J.F. Carrier, S. Bedwani, H. Bouchard, Robust quantitative contrast-enhanced dual-energy CT for radiotherapy applications, Med. Phys. 45 (7) (2018) 3086–3096.
[28] A. Lalonde, H. Bouchard, A general method to derive tissue parameters for Monte Carlo dose calculation with multi-energy CT, Phys. Med. Biol. 61 (22) (2016) 8044–8069.
[29] M.R. Issa, S.E. Samuels, E. Bellile, F.L. Shalabi, A. Eisbruch, G. Wolf, Tumor volumes and prognosis in laryngeal Cancer, Cancers (Basel) 7 (4) (2015) 2236–2261.
[30] T.J. Vrtiska, N. Takahashi, J.G. Fletcher, R.P. Hartman, L. Yu, A. Kawashima, Genitourinary applications of dual-energy CT, AJR Am. J. Roentgenol. 194 (6) (2010) 1434–1442.
[31] G. Schmid-Bindert, T. Henzler, T.Q. Chu, M. Meyer, J.W. Nance Jr., U.J. Schoepf, et al., Functional imaging of lung cancer using dual energy CT: how does iodine related attenuation correlate with standardized uptake value of 18FDG-PET-CT? Eur. Radiol. 22 (1) (2012) 93–103.
[32] R. Hermans, P. Lambin, A. Van der Goten, W. Van den Bogaert, B. Verbist, C. Weltens, et al., Tumoural perfusion as measured by dynamic computed tomography in head and neck carcinoma, Radiother. Oncol. 53 (2) (1999) 105–111.
[33] R.J. Gillies, P.A. Schornack, T.W. Secomb, N. Raghunand, Causes and effects of heterogeneous perfusion in tumors, Neoplasia 1 (3) (1999) 197–207.
[34] S.M. Eschmann, F. Paulsen, M. Reimold, H. Dittmann, S. Welz, G. Reischl, et al., Prognostic impact of hypoxia imaging with 18F-misonidazole PET in non-small cell lung cancer and head and neck cancer before radiotherapy, J. Nucl. Med. 46 (2) (2005) 253–260.
[35] D. Thorwarth, S.M. Eschmann, J. Scheiderbauer, F. Paulsen, M. Alber, Kinetic analysis of dynamic 18F-fluoromisonidazole PET correlates with radiation treatment outcome in head-and-neck cancer, BMC Cancer 5 (2005) 152.
[36] K. Lehtio, O. Eskola, T. Viljanen, V. Oikonen, T. Gronroos, L. Sillanmaki, et al., Imaging perfusion and hypoxia with PET to predict radiotherapy response in head-and-neck cancer, Int. J. Radiat. Oncol. Biol. Phys. 59 (4) (2004) 971–982.
[37] N.L. Hoefling, J.B. McHugh, E. Light, B. Kumar, H. Walline, M. Prince, et al., Human papillomavirus, p16, and epidermal growth factor receptor biomarkers and CT perfusion values in head and neck squamous cell carcinoma, AJNR Am. J. Neuroradiol. 34 (5) (2013) s1–s2 1062-6.
[38] C. Pietsch, F. de Galiza Barbosa, M.W. Hullner, D.T. Schmid, S.K. Haerle, G.F. Huber, et al., Combined PET/CT-perfusion in patients with head and neck cancers might predict failure after radio-chemotherapy: a proof of concept study, BMC Med. Imaging 15 (2015) 60.
[39] L. Hlatky, P. Hahnfeldt, J. Folkman, Clinical application of antiangiogenic therapy: microvessel density, what it does and doesn't tell us, J. Natl. Cancer Inst. 94 (12) (2002) 883–893.
[40] P. Carmeliet, R.K. Jain, Molecular mechanisms and clinical applications of angiogenesis, Nature 473 (7347) (2011) 298–307.
[41] S. Bisdas, K. Spicer, Z. Rumboldt, Whole-tumor perfusion CT parameters and glucose metabolism measurements in head and neck squamous cell carcinomas: a pilot study using combined positron-emission tomography/CT imaging, AJNR Am. J. Neuroradiol. 29 (7) (2008) 1376–1381.
[42] J.F. Jansen, Y. Lu, G. Gupta, N.Y. Lee, H.E. Stambuk, Y. Mazaheri, et al., Texture analysis on parametric maps derived from dynamic contrast-enhanced magnetic resonance imaging in head and neck cancer, World J. Radiol. 8 (1) (2016) 90–97.
[43] S. Ursino, L. Faggioni, F. Fiorica, D. Delishaj, V. Seccia, F. Pasqualetti, et al., Role of perfusion CT in the evaluation of metastatic nodal tumor response after radiochemotherapy in head and neck cancer: preliminary findings, Eur. Rev. Med. Pharmacol. Sci. 21 (21) (2017) 4882–4890.
[44] A. Shukla-Dave, N.Y. Lee, J.F. Jansen, H.T. Thaler, H.E. Stambuk, M.G. Fury, et al., Dynamic contrast-enhanced magnetic resonance imaging as a predictor of outcome in head-and-neck squamous cell carcinoma patients with nodal metastases, Int. J. Radiat. Oncol. Biol. Phys. 82 (5) (2012) 1837–1844.
[45] Y. Cao, A. Popovtzer, D. Li, D.B. Chepeha, J.S. Moyer, M.E. Prince, et al., Early prediction of outcome in advanced head-and-neck cancer based on tumor blood volume alterations during therapy: a prospective study, Int. J. Radiat. Oncol. Biol. Phys. 72 (5) (2008) 1287–1290.
[46] W. van Elmpt, G. Landry, M. Das, F. Verhaegen, Dual energy CT in radiotherapy: current applications and future outlook, Radiother. Oncol. 119 (1) (2016) 137–144.